metals

MDPI

Article

Effect of Ta Content on Scratching Behavior of Ti-Al-Ta-N Coatings on Titanium Substrate

Artur Shugurov * and Evgenii Kuzminov

Institute of Strength Physics and Material Science, Siberian Branch of the Russian Academy of Science, Akademicheskii pr. 2/4, 634055 Tomsk, Russia; evgenij_kuzminov00@mail.ru

* Correspondence: shugurov@ispms.ru

Abstract: The effect of Ta alloying on the structure, mechanical properties and scratching behavior of Ti-Al-N-based coatings deposited on Ti substrates by reactive direct-current magnetron sputtering is studied. It was found that increasing the Ta content in the $Ti_{1-x-y}Al_xTa_yN$ coatings from $y = 0$ to $y = 0.65$ led to a decrease in hardness and Young's modulus but an increase in the hardness-to-modulus ratio. This resulted in the reduction of the load-bearing capacity of the Ta-alloyed coatings and enhancement of their toughness. The competition among these trends determined the improved crack resistance and adhesion of the $Ti_{0.31}Al_{0.34}Ta_{0.35}N$ coating under scratching.

Keywords: Ti-Al-Ta-N coatings; titanium; scratching

check for updates

Citation: Shugurov, A.; Kuzminov, E. Effect of Ta Content on Scratching Behavior of Ti-Al-Ta-N Coatings on Titanium Substrate. *Metals* **2022**, *12*, 1017. https://doi.org/10.3390/met12061017

Academic Editor: Changdong Gu

Received: 27 May 2022
Accepted: 14 June 2022
Published: 15 June 2022

Publisher's Note: MDPI stays neutral with regard to jurisdictional claims in published maps and institutional affiliations.

1. Introduction

Titanium and its alloys are increasingly used in aerospace and mechanical engineering, marine applications, power generation, chemical industries, medicine, etc. This is due to the high strength-to-weight ratio, low heat conductivity, corrosion resistance and biocompatibility of these materials [1–3]. However, in many applications, the titanium components must operate under severe wear conditions, although it has long been recognized that titanium suffers from poor wear resistance when rubbed against different materials [4,5]. Therefore, the surface modification of the components is needed to significantly improve their tribological performance [6].

One of the most widely used ways to enhance the surface hardness and wear resistance of titanium parts is to coat them with hard protective layers [7,8]. Among these, Ti-Al-N coatings have attracted considerable attention due to the face of their superior hardness, wear and oxidation resistance [9–14]. It has been shown that even more enhanced mechanical and tribological performance of the Ti-Al-N coatings can be achieved by their alloying with additional elements (V, Cr, Y, Nb, Ta, Si, etc.) [15–17]. In particular, ab initio calculations have predicted that substitutional incorporation of VB and VIB elements into the metal sublattice of Ti-Al-N-based quaternary solid solutions leads to enhanced occupancy of d-t_{2g} metallic states [18,19]. This should provide significant toughening of the quaternaries compared with Ti-Al-N coatings, which inherent brittleness facilitates their cracking and delamination under contact loads, thereby significantly reducing the wear resistance. These theoretical predictions have been supported by experimental results. A recent study of magnetron-sputtered Ti-Al-Ta-N coatings on titanium substrates has shown that their fracture toughness exhibited an increasing trend with an increase in the Ta content [20]. However, the increase in toughness of the Ti-Al-Ta-N coatings was accompanied by a decrease in their hardness and Young's modulus. In the case of a soft titanium substrate, this can result in a reduction in the load-bearing capacity of the coating/substrate system, i.e., a decrease in the allowable applied normal load, beyond which the plastic flow of the substrate material causes large bending deformation of the coating followed by its catastrophic failure [21]. Therefore, in order to optimize the Ta content of the Ti-Al-Ta-N

coatings for tribological applications, it is necessary to study the influence of Ta alloying on the mechanical performance of the coating/substrate system under contact loading. This work focused on the effect of the Ta content on the scratching behavior of Ti-Al-Ta-N coatings on titanium substrates.

2. Materials and Methods

$Ti_{1-x-y}Al_xTa_yN$ coatings were deposited onto commercially pure titanium and Si (100) substrates. The coatings on the Si substrates were used for the measurement of the residual stress as well as for examination of fractured cross-sections. Other experiments were performed with the coatings sputtered on the Ti substrates. The substrates were sputter-cleaned with Ar^+ ions followed by deposition of a 30 nm thick TiAl adhesion layer by DC magnetron sputtering. The coatings were deposited by DC magnetron co-sputtering using two planar magnetrons with Ti/Al (55/45 at.%) and Ta (99.99%) targets. The power density at the Ti/Al target was 11.4 W/cm^2, while at the Ta target it was varied from 3.8 to 12.7 W/cm^2. The sputtering was carried out in a mixed Ar + N_2 atmosphere at a total pressure of 0.3 Pa, while the partial pressure of nitrogen was kept at 0.06 Pa. The coatings were deposited onto grounded substrates heated to 425 °C. The coating thickness was 3.0 μm.

The microstructural characterization of the coatings in the cross-section geometry and determination of their elemental composition using energy-dispersive X-ray spectroscopy (EDS) were carried out with an LEO EVO 50 scanning electron microscope (SEM, Carl Zeiss, Jena, Germany). The phase composition of the coatings was investigated by X-ray diffraction (XRD) in the Bragg–Brentano configuration using an XRD-7000 diffractometer (Shimadzu, Kyoto, Japan; the equipment belonged to the Share Use Center for "Nanomaterials and nanotechnologies" at the Tomsk Polytechnic University, supported by the RF Ministry of Education and Science; project no. 075-15-2021-710) with CuKα radiation (λ = 1.5406 Å). The residual stresses (σ) were extracted from the substrate curvature measurements. The hardness (H) and Young's modulus (E) were determined by nanoindentation with a NanoTest system (version, Micro Materials Ltd., Wrexham, UK) using a Berkovich diamond at a maximum applied load of 20 mN. The scratch tests were performed with a Revetest instrument (CSM instruments, Peseux, Switzerland) using a conical Rockwell indenter with a tip curvature radius of 200 μm. The scratches were made 7 mm long with a sliding speed of 2 mm/min. The maximum applied load was 55 N. The variations in the friction coefficient and acoustic emission signals were recorded during the tests. The examination of the scratch grooves was performed using an Axiovert 40 Mat optical microscope (Carl Zeiss, Jena, Germany).

3. Results

The chemical compositions of the $Ti_{1-x-y}Al_xTa_yN$ coatings determined from the EDS analysis are listed in Table 1. The Ta content in the coatings varied from $y = 0$ to $y = 0.65$. Figure 1 exhibits X-ray diffraction patterns of the coatings, which reveal a single-phase B1-type fcc crystal structure of the $Ti_{0.45}Al_{0.55}N$ and $Ti_{1-x-y}Al_xTa_yN$ solid solutions. It can be seen from Figure 1 that the increase in the Ta content led to shifts in the XRD peaks to lower diffraction angles that corresponded to an increase in the lattice constant from 0.417 nm for $Ti_{0.45}Al_{0.55}N$ to 0.434 nm for $Ti_{0.20}Al_{0.15}Ta_{0.65}N$. This was due to the fact that the lattice constant of the fcc TaN phase (0.434 nm) was significantly larger than those of the TiN phase (0.424 nm) and the fcc AlN phase (0.412 nm). The other consequence of the increase in the Ta content of the coatings was their crystallographic texture evolution. While the $Ti_{0.45}Al_{0.55}N$ coating had strong (111) preferential orientation in the growth direction, the XRD pattern of the $Ti_{0.20}Al_{0.15}Ta_{0.65}N$ coating exhibited a very strong (200) texture.

Table 1. Mechanical properties of the $Ti_{1-x-y}Al_xTa_yN$ coatings.

Coating	H, GPa	E, GPa	H/E	σ, GPa	h_r, Nm
$Ti_{0.45}Al_{0.55}N$	31.2 ± 1.3	463 ± 18	0.067	−1.6	300 ± 7
$Ti_{0.41}Al_{0.49}Ta_{0.10}N$	30.4 ± 1.1	434 ± 20	0.070	−3.0	312 ± 19
$Ti_{0.37}Al_{0.43}Ta_{0.20}N$	29.2 ± 1.4	399 ± 18	0.073	−3.5	322 ± 16
$Ti_{0.31}Al_{0.34}Ta_{0.35}N$	30.9 ± 1.2	373 ± 19	0.083	−3.9	310 ± 10
$Ti_{0.27}Al_{0.28}Ta_{0.45}N$	29.1 ± 1.2	368 ± 18	0.079	−3.7	324 ± 18
$Ti_{0.20}Al_{0.15}Ta_{0.65}N$	28.3 ± 1.2	351 ± 15	0.081	−2.1	352 ± 14

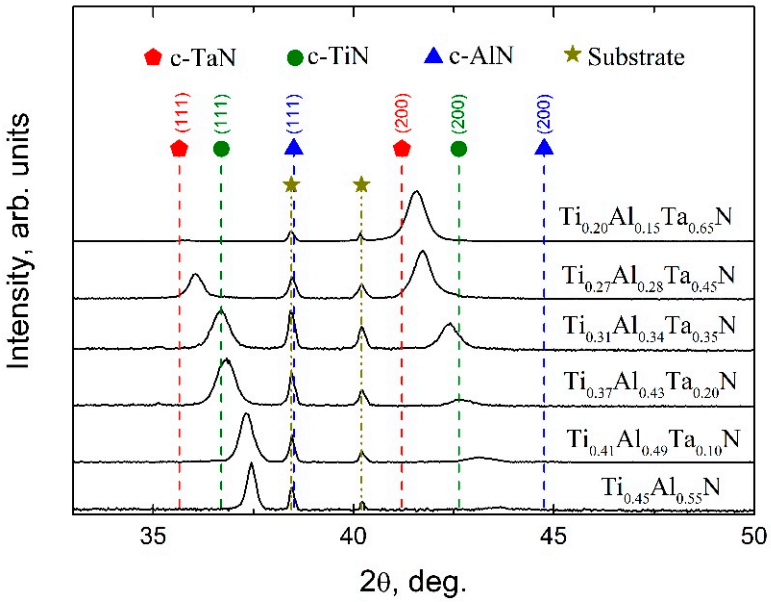

Figure 1. X-ray diffraction patterns of the $Ti_{1-x-y}Al_xTa_yN$ coatings with different Ta contents.

In order to quantitatively characterize the textural evolution in the $Ti_{1-x-y}Al_xTa_yN$ coatings, the texture coefficient (*TC*) was calculated for the (111) and (200) crystal planes from the following equation [22]:

$$TC_{hkl} = \frac{\frac{I_{hkl}}{I_{0hkl}}}{\frac{1}{n}\sum_n \left(\frac{I_{hkl}}{I_{0hkl}}\right)} \quad (1)$$

where I_{hkl} is the measured intensity of the XRD peak corresponding to the (*hkl*) plane for the phase; I_{ohkl} is the intensity of the same XRD peak of a standard reference sample; $n = 2$ is the number of used XRD peaks. The texture coefficients for the (111) and (200) crystal planes, calculated using the reference data for TiN (JCPDS-ICDD No. 38-1420), are shown in Figure 2 as a function of the Ta content in the coatings y. It can be seen that the *TC* for the (111) plane decreased with an increase in y. The *TC* decreased rather slowly at $y < 0.35$, while at higher Ta contents, it dropped significantly faster. The texture coefficient for the (200) plane exhibited the opposite behavior.

Figure 3 shows SEM micrographs of the fracture cross-sections of the $Ti_{1-x-y}Al_xTa_yN$ coatings on Si substrates. The images show that the coatings had a dense columnar microstructure. It can also be seen that the samples with low Ta contents ($y < 0.35$) were characterized by V-shaped grains, which usually form under competitive grain growth [23]. Considering the XRD results, it can be thought that the coatings started to grow from the nucleation of crystallites with different crystallographic orientations, but the (111) crystallites dominated the subsequent growth. In contrast, the straight columnar grains with parallel boundaries extending through the whole coating thickness formed at high Ta contents ($y \geq 0.35$), when the preferred orientation of grains changed from (111) to

(200). This means that the columnar grains in these coatings primarily resulted from the concurrent growth of nuclei initially formed on the substrate rather than from the dominant growth of favorably oriented grains, which survived at the expense of adjacent crystallites.

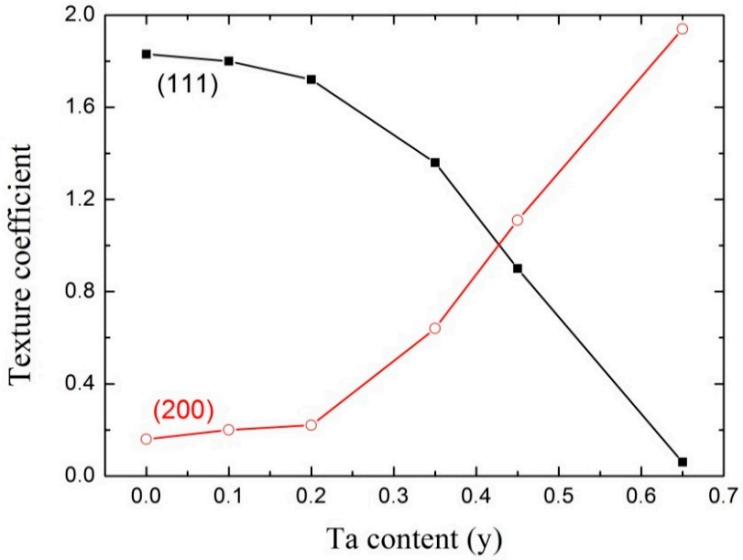

Figure 2. Texture coefficient of the $Ti_{1-x-y}Al_xTa_yN$ coatings as a function of the Ta content *y*.

As can be seen from Table 1, all these coatings were characterized by compressive residual stresses. The stresses initially increased with an increase in the Ta content from −1.6 GPa in $Ti_{0.45}Al_{0.55}N$ to −3.9 GPa in $Ti_{0.31}Al_{0.34}Ta_{0.35}N$ and dropped thereafter to −2.1 GPa in $Ti_{0.20}Al_{0.15}Ta_{0.65}N$. The evolution of the residual stresses can shed light on the origin of the structural changes. From a thermodynamic point of view, high strains (stresses) should favor the (111) texture to form in TiN-based coatings [24,25]. However, this was not the case in the $Ti_{1-x-y}Al_xTa_yN$ coatings, which demonstrated a decrease in the degree of the (111) texture with the increase in the residual stresses at *y* varying from 0 to 0.35. The textural changes in the TiN-based coatings can also be induced by kinetic factors, namely, changes in the mobility of adatoms and the probability of their re-sputtering which, in turn, are governed by deposition parameters such as substrate temperature, ion flux and substrate bias [26,27]. However, the only deposition parameter that varied in the present study was the Ta target power density. An increase in the power density obviously results in an increase in the Ta flux. Meanwhile, it was found that an increase in the flux of metal species favored a (111)-oriented growth of the TiN-based coatings [26]. Therefore, it can be assumed that it was a growing number of Ta atoms incorporated into the TiN-based lattice that gave rise to changing the preferred orientation of the $Ti_{1-x-y}Al_xTa_yN$ coatings from (111) to (200).

The Ta atoms were characterized by a larger atomic volume in the TiN-based cubic crystal structure that manifested itself in the abovementioned increase in the lattice constant of the $Ti_{1-x-y}Al_xTa_yN$ solid solution with the increase in the Ta content. Consequently, incorporation of Ta atoms into the TiN lattice resulted in its distortions, which induced the elastic strains of the coatings. However, the coatings could change only their out-of-plane dimension, while the lateral dimensions were fixed owing to constraints superimposed by the substrate due to the rigid bonding at the interface. The latter led to the development of compressive in-plane stresses in the coatings. Evidently, the stresses should be larger, when the (111) plane is parallel to the interface, because it is the most close-packed plane in the fcc structure. The less close-packed (200) plane provided easier accommodation of the Ta atoms and lower stresses. Therefore, in terms of the minimization of the strain energy with a greater Ta content in the coatings, the more unfavorable the growth of (111) grains. As a result, high Ta contents led to the formation of the (200) preferred orientation, which provided a significant reduction in the residual compressive stresses.

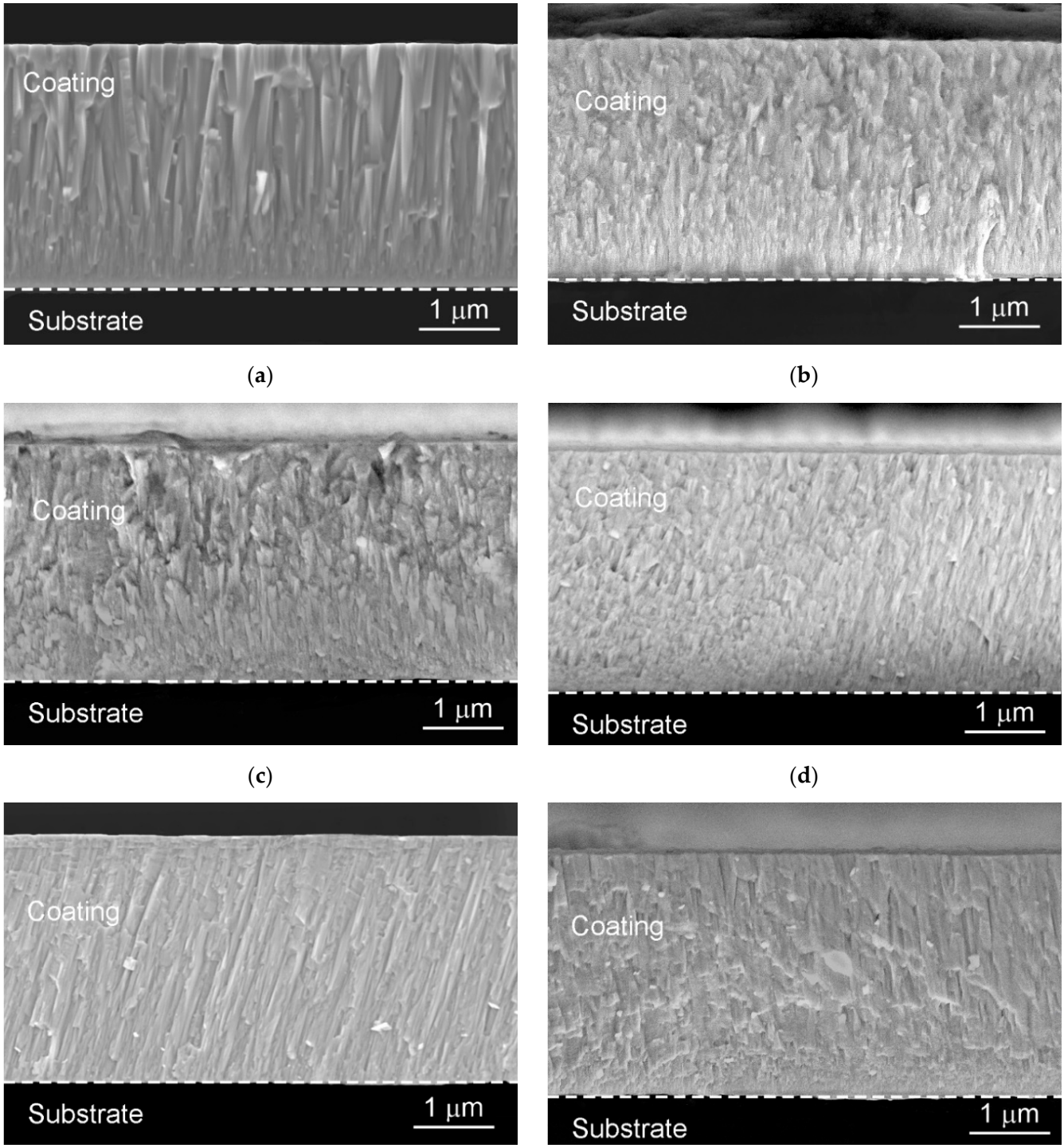

Figure 3. Cross-sectional SEM micrographs of (**a**) $Ti_{0.45}Al_{0.55}N$; (**b**) $Ti_{0.41}Al_{0.49}Ta_{0.10}N$; (**c**) $Ti_{0.37}Al_{0.43}Ta_{0.20}N$; (**d**) $Ti_{0.31}Al_{0.34}Ta_{0.35}N$; (**e**) $Ti_{0.27}Al_{0.28}Ta_{0.45}N$; (**f**) $Ti_{0.20}Al_{0.15}Ta_{0.65}N$ coatings on Si substrates.

The mechanical characteristics of the coatings are listed in Table 1. Both the hardness and Young's modulus exhibited an overall decreasing trend with an increase in the Ta content. However, in contrast to the Young's modulus, which continuously dropped, the hardness demonstrated a local peak at $y = 0.35$. This can be attributed to the fact that the $Ti_{0.31}Al_{0.34}Ta_{0.35}N$ coating was characterized by the highest compressive stress, which

contributed to the increase in hardness. As a result, the H/E ratio, which is often used to rank the ductility and toughness of hard coatings, also exhibited a peak value at $y = 0.35$.

The residual depth (h_r) of the indentation imprints on the coating surface obtained at a load of 100 mN was determined to characterize the load-bearing capacity of the coating/substrate system. At this load, the penetration depth of the indenter into the coatings reached ~480 nm, and the measured hardness started to decrease due to the contribution of the indentation response from the softer Ti substrate caused by its plastic flow. Obviously, in the samples with the lower load-bearing capacity, the substrate was subjected to greater plastic deformation that significantly contributed to the deeper residual imprints. The h_r values given in Table 1 indicate that the $Ti_{0.45}Al_{0.55}N$ coating provided the highest load-bearing capacity due to the high H and E values. The $Ti_{0.20}Al_{0.15}Ta_{0.65}N$ coating expectedly demonstrated the lowest load-bearing capacity.

Figure 4 presents the results of the scratch testing of the coatings. The friction coefficient and acoustic emission signal are shown as a function of the scratch length and applied load. The scratch micrographs and critical loads corresponding to the first crack event (L_{c1}) and the massive spallation of the coatings (L_{c2}) are also displayed. As is usual for compliant Ti substrates [28], the indenter movement resulted in the formation of grooves due to the ploughing of the substrate with coherent bending of the $Ti_{1-x-y}Al_xTa_yN$ coatings. Microscopic examination of the scratches revealed, in all coatings, parallel and angular cracks at the groove flanks as well as tensile and conformal transverse cracks inside the grooves. With increasing load, the cracks penetrated through the coating thickness, resulting in recovery and buckling spallation of the coating fragments. The cracks had sloping sides; therefore, the chipping primarily occurred with no or small areas of substrate exposure. Finally, massive spallation of most of the coatings was observed, which was accompanied by an increasing friction coefficient due to the contact between the indenter and Ti substrate. It can be seen from Figure 4 that all $Ti_{1-x-y}Al_xTa_yN$ coatings started to crack at higher loads than the $Ti_{0.45}Al_{0.55}N$ coating. Most of the $Ti_{1-x-y}Al_xTa_yN$ coatings were characterized by close L_{c1} values (~10 N), except for $Ti_{0.31}Al_{0.34}Ta_{0.35}N$, where cracking occurred at a noticeably higher load of 13.4 N. The latter can be attributed to the combination of the high toughness, load-bearing capacity and compressive stress in the latter coating, which suppressed crack initiation and propagation. In addition, all of the Ta-alloyed coatings had higher L_{c2} values than $Ti_{0.45}Al_{0.55}N$. However, in contrast to L_{c1}, the L_{c2} load increased with the Ta content up to $y = 0.35$ and dropped thereafter.

The improved adhesion of the $Ti_{0.31}Al_{0.34}Ta_{0.35}N$ coating can mainly be attributed to the combination of high toughness and load-bearing capacity. Obviously, the tougher coating resists longer against propagation of the through-thickness cracks and their deflection at the coating/substrate interface, which led to delamination and the total removal of the coatings from the scratch groove. Therefore, the coatings with high Ta contents ($y \geq 0.35$), which were characterized by enhanced toughness, should demonstrate better adhesion than the coatings with $y < 0.35$. However, the $Ti_{0.27}Al_{0.28}Ta_{0.45}N$ and especially the $Ti_{0.20}Al_{0.15}Ta_{0.65}N$ coatings exhibited a decreased load-bearing capacity compared with $Ti_{0.31}Al_{0.34}Ta_{0.35}N$. The reduction of the load-bearing capacity resulted in a higher penetration depth of the stylus into the samples. The latter caused more substrate material to be displaced from the groove, and larger pile-ups formed at the scratch flanks and ahead of the moving stylus. The large pile-ups resulted in stronger bending of the coatings, facilitating nucleation and propagation of through-thickness cracks and, consequently, coating delamination. Therefore, the $Ti_{0.27}Al_{0.28}Ta_{0.45}N$ and $Ti_{0.20}Al_{0.15}Ta_{0.65}N$ coatings demonstrated lower L_{c2} loads than $Ti_{0.31}Al_{0.34}Ta_{0.35}N$.

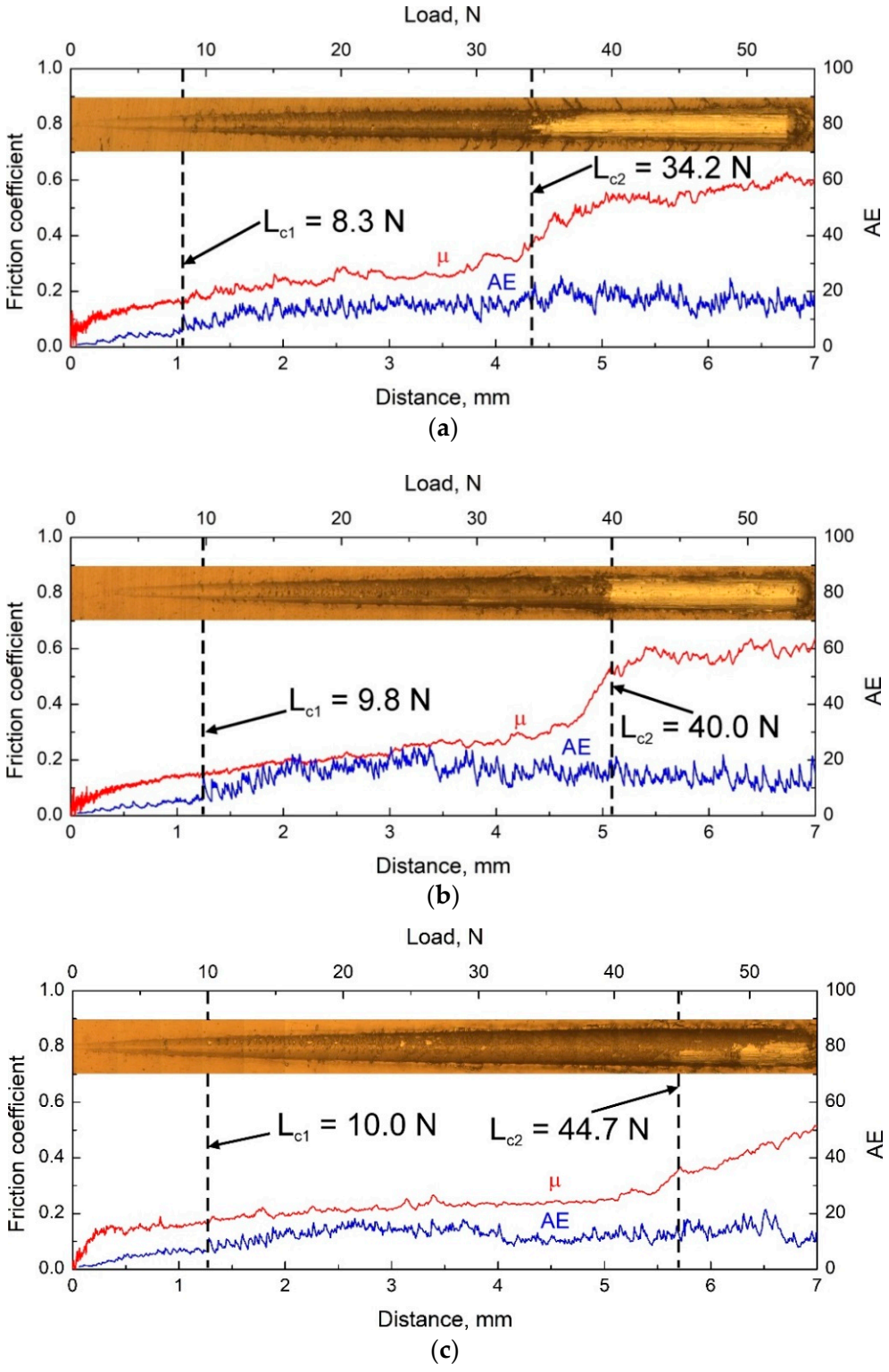

Figure 4. *Cont.*

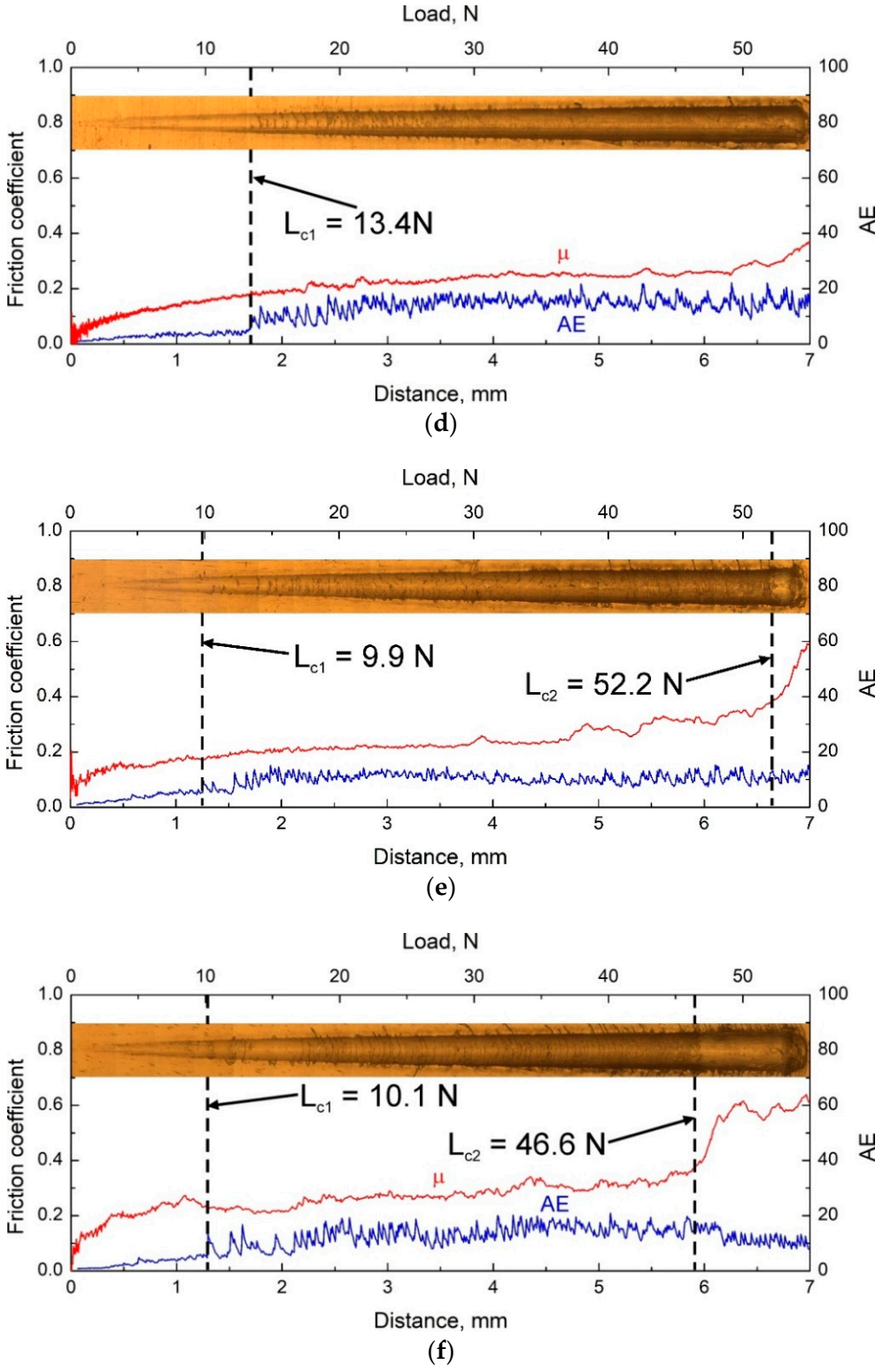

Figure 4. Scratch tracks, friction coefficients (μ), acoustic emission signals (AE) and critical loads of the (**a**) $Ti_{0.45}Al_{0.55}N$; (**b**) $Ti_{0.41}Al_{0.49}Ta_{0.10}N$; (**c**) $Ti_{0.37}Al_{0.43}Ta_{0.20}N$; (**d**) $Ti_{0.31}Al_{0.34}Ta_{0.35}N$; (**e**) $Ti_{0.27}Al_{0.28}Ta_{0.45}N$; (**f**) $Ti_{0.20}Al_{0.15}Ta_{0.65}N$ coatings.

Considering the above discussion, it is reasonable to suppose that the critical load L_{c2} was proportional to the H/E ratio, which characterizes the coating toughness, and inversely proportional to the residual indentation depth (h_r), which represents the load-bearing capacity. Thus, the ratio of H/E to h_r can be used to describe the observed variations

in the L_{c2} load. Figure 5a exhibits the $(H/E)/h_r$ ratio as a function of the Ta content (y) in the $Ti_{1-x-y}Al_xTa_yN$ coatings. It was observed that at low Ta contents ($y < 0.35$), the $(H/E)/h_r$ ratio weakly increased due to the coating toughening, despite a decrease in the load-bearing capacity. The concomitant increase in H/E and decrease in h_r led to a sharp increase in their ratio in the $Ti_{0.31}Al_{0.34}Ta_{0.35}N$ coating. At a higher y, the $(H/E)/h_r$ ratio dropped owing to the decreasing load-bearing capacity. Figure 5b demonstrates the critical load L_{c2} vs. the $(H/E)/h_r$ ratio for the $Ti_{1-x-y}Al_xTa_yN$ coatings. As expected, the overall increasing trend of the L_{c2} is clearly visible. However, two distinct areas of change in the critical load, approximated by lines 1 and 2, can be distinguished. In the first area, which was located at low $(H/E)/h_r$ values and corresponded to the coatings with low Ta contents ($y < 0.35$), L_{c2} exhibited rapid growth. The second area, which belonged to the coatings with $y \geq 0.35$, was characterized by a significantly smaller slope of the approximating line. Considering the above discussion, the increase in L_{c2} in area 1 can be attributed to the toughening of the coatings caused by their alloying with Ta, which suppressed crack propagation and coating delamination. The increasing trend of L_{c2} at higher $(H/E)/h_r$ ratios (area 2) did not correlate with the coating toughness, but well agreed with the increase in their load-bearing capacity. The different slopes of lines 1 and 2 indicate the different tribomechanical behaviors of the $Ti_{1-x-y}Al_xTa_yN$ coatings with low and high Ta contents. This means that there were additional factors that deteriorated the scratching performance of the coatings at $y \geq 0.35$. Considering the results of the XRD and SEM studies of the $Ti_{1-x-y}Al_xTa_yN$ coatings, it can be concluded that these factors were concerned with the structural changes of the coatings with the high Ta contents, namely, the formation of the (200) texture and straight columnar grains extending through the whole coating thickness. It has been shown that the (200) texturized TiN-based coatings are characterized by a lower wear resistance than those exhibiting the preferred (111) orientation [29]. The straight boundaries of the columnar grains significantly facilitate propagation of through-thickness cracks, which promote coating delamination.

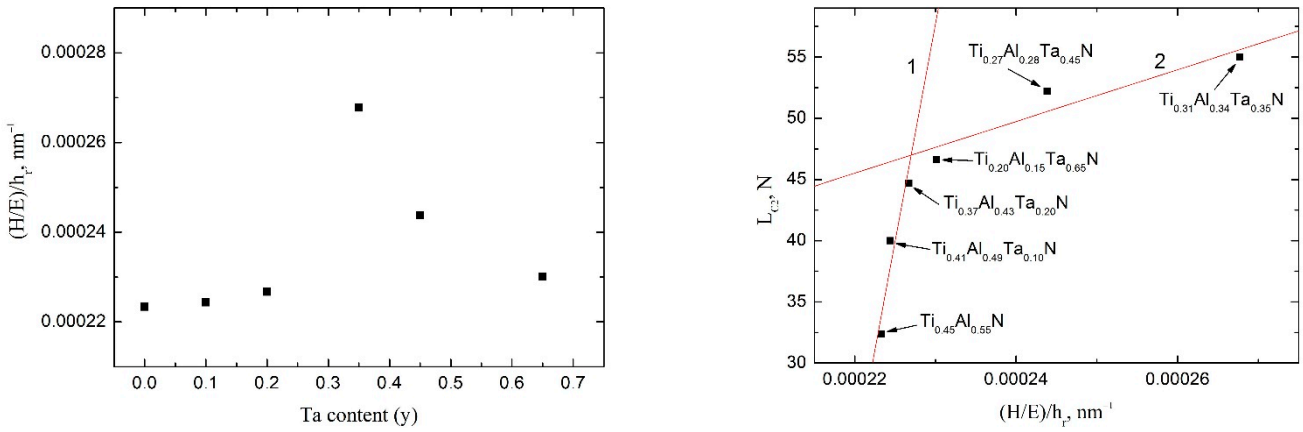

Figure 5. (**a**) $(H/E)/h_r$ ratio vs. Ta content (y) in the $Ti_{1-x-y}Al_xTa_yN$ coatings; (**b**) critical load for the massive spallation of the $Ti_{1-x-y}Al_xTa_yN$ coatings as a function of the $(H/E)/h_r$ ratio.

4. Conclusions

Alloying of Ti-Al-N coatings with Ta was shown to result in their toughening, on the one hand, and in a decreasing trend in their load-bearing capacity, on the other hand. In addition, incorporation of Ta atoms into the Ti-Al-N lattice led to the enhancement of residual compressive stresses in the $Ti_{1-x-y}Al_xTa_yN$ coatings with an increase in the Ta content up to $y = 0.35$. The latter provided local peaks in the hardness and load-bearing capacity of the $Ti_{0.31}Al_{0.34}Ta_{0.35}N$ coating. Due to the beneficial combination of the increased toughness and reasonably high load-bearing capacity, the $Ti_{0.31}Al_{0.34}Ta_{0.35}N$

coating exhibited the highest crack resistance and adhesion when the scratching of the coatings with the Ta contents y varied from 0 to 0.65.

Author Contributions: Conceptualization, A.S.; methodology, A.S.; investigation, E.K. and A.S.; writing—original draft preparation, A.S.; visualization, E.K.; writing—review and editing, A.S. All authors have read and agreed to the published version of the manuscript.

Funding: This work was performed according to a government research assignment for ISPMS SB RAS (project no. FWRW-2021–0010).

Institutional Review Board Statement: Not applicable.

Informed Consent Statement: Not applicable.

Data Availability Statement: The data presented in this study are available upon request from the corresponding author.

Acknowledgments: The investigations were carried out using the equipment of the Share Use Center "Nanotech" of the ISPMS SB RAS.

Conflicts of Interest: The authors declare no conflict of interest.

References

1. Leyens, C.; Peters, M. *Titanium and Titanium Alloys*; Wiley-VCH: Weinheim, Germany, 2003; ISBN 9783527305346.
2. Lütjering, G.; Williams, J.C. *Titanium*, 2nd ed.; Springer: Berlin/Heidelberg, Germany, 2007; ISBN 978-3-540-71397-5.
3. Froes, F.H. *Titanium: Physical Metallurgy, Processing, and Applications*; EngineeringPro Collection; ASM International: Materials Park, OH, USA, 2015; ISBN 9781627080804.
4. Miller, P.D.; Holladay, J.W. Friction and wear properties of titanium. *Wear* **1958**, *2*, 133–140. [CrossRef]
5. Qu, J.; Blau, P.J.; Watkins, T.R.; Cavin, O.B.; Kulkarni, N.S. Friction and wear of titanium alloys sliding against metal, polymer, and ceramic counter faces. *Wear* **2005**, *258*, 1348–1356. [CrossRef]
6. Panin, V.E.; Ovechkin, B.B.; Khayrullin, R.R.; Lider, A.M.; Bordulev, Y.S.; Panin, A.V.; Perevalova, O.B.; Vlasov, I.V. Effect of the lattice curvature of Ti-6Al-4V titanium alloy on their fatigue life and fracture toughness. *Phys. Mesomech.* **2020**, *23*, 369–375. [CrossRef]
7. Bai, H.; Zhong, L.; Kang, L.; Liu, J.; Zhuang, W.; Lv, Z.; Xu, Y. A Review on wear-resistant coating with high hardness and high toughness on the surface of titanium alloy. *J. Alloys Compd.* **2021**, *882*, 160645. [CrossRef]
8. Valiev, R.R.; Modina, Y.M.; Selivanov, K.S.; Semenova, I.P.; Khafizova, E.D.; Valiev, R.Z.; Savina, Y.N. Enhanced service properties of a protective coating on a titanium alloy with an ultrafine-grained structure. *Mater. Lett.* **2021**, *305*, 130781. [CrossRef]
9. Yildiz, F.; Yetim, A.F.; Alsaran, A.; Çelik, A.; Kaymaz, I.; Efeoğlu, I. Plain and fretting fatigue behavior of Ti6Al4V alloy coated with TiAlN thin film. *Tribol. Int.* **2013**, *66*, 307–314. [CrossRef]
10. Yi, P.; Peng, L.; Huang, J. Multilayered TiAlN Films on Ti6Al4V alloy for biomedical applications by closed field unbalanced magnetron sputter ion plating process. *Mater. Sci. Eng. C* **2016**, *59*, 669–676. [CrossRef]
11. Niu, R.; Li, J.; Wang, Y.; Chen, J.; Xue, Q. Structure and high temperature tribological behavior of TiAlN/Nitride duplex treated coatings on Ti6Al4V. *Surf. Coat. Technol.* **2017**, *309*, 232–241. [CrossRef]
12. Shulepov, I.A.; Kashkarov, E.B.; Stepanov, I.B.; Syrtanov, M.S.; Sutygina, A.N.; Shanenkov, I.; Obrosov, A.; Weiß, S. The formation of composite Ti-Al-N coatings using filtered vacuum arc deposition with separate cathodes. *Metals* **2017**, *7*, 497. [CrossRef]
13. Sousa, V.F.C.; da Silva, F.J.G.; Pinto, G.F.; Baptista, A.; Alexandre, R. Characteristics and wear mechanisms of TiAlN-based coatings for machining applications: A comprehensive review. *Metals* **2021**, *11*, 260. [CrossRef]
14. Shugurov, A.R.; Panin, A.V.; Dmitriev, A.I.; Nikonov, A.Y. Multiscale fracture of Ti-Al-N coatings under uniaxial tension. *Phys. Mesomech.* **2021**, *24*, 185–195. [CrossRef]
15. Chen, Y.H.; Roa, J.J.; Yu, C.H.; Johansson-Jõesaar, M.P.; Andersson, J.M.; Anglada, M.J.; Odén, M.; Rogström, L. Enhanced thermal stability and fracture toughness of TiAlN coatings by Cr, Nb and V-alloying. *Surf. Coat. Technol.* **2018**, *342*, 85–93. [CrossRef]
16. Aninat, R.; Valle, N.; Chemin, J.B.; Duday, D.; Michotte, C.; Penoy, M.; Bourgeois, L.; Choquet, P. Addition of Ta and Y in a hard Ti-Al-N PVD coating: Individual and conjugated effect on the oxidation and wear properties. *Corros. Sci.* **2019**, *156*, 171–180. [CrossRef]
17. Li, G.; Li, L.; Han, M.; Luo, S.; Jin, J.; Wang, L.; Gu, J.; Miao, H. The performance of TiAlSiN coated cemented carbide tools enhanced by inserting Ti interlayers. *Metals* **2019**, *9*, 918. [CrossRef]
18. Sangiovanni, D.G.; Chirita, V.; Hultman, L. Toughness enhancement in TiAlN-based quarternary alloys. *Thin Solid Film.* **2012**, *520*, 4080–4088. [CrossRef]
19. Mikula, M.; Plašienka, D.; Sangiovanni, D.G.; Sahul, M.; Roch, T.; Truchlý, M.; Gregor, M.; Čaplovič, L.; Plecenik, A.; Kúš, P. Toughness enhancement in highly NbN-alloyed Ti-Al-N hard coatings. *Acta Mater.* **2016**, *121*, 59–67. [CrossRef]
20. Shugurov, A.R.; Kuzminov, E.D.; Kasterov, A.M.; Panin, A.V.; Dmitriev, A.I. Tuning of mechanical properties of $Ti_{1-x}Al_xN$ coatings through Ta alloying. *Surf. Coat. Technol.* **2020**, *382*, 125219. [CrossRef]

21. Kot, M.; Rakowski, W.; Major, Ł.; Lackner, J. Load-bearing capacity of coating–substrate systems obtained from spherical indentation tests. *Mater. Des.* **2013**, *46*, 751–757. [CrossRef]
22. Xian, G.; Zhao, H.-B.; Fan, H.-Y.; Du, H. Structure and mechanical properties of Zr/TiAlN films prepared by plasma-enhanced magnetron sputtering. *Rare Met.* **2015**, *34*, 717–724. [CrossRef]
23. Abadias, G. Stress and preferred orientation in nitride-based PVD coatings. *Surf. Coat. Technol.* **2008**, *202*, 2223–2235. [CrossRef]
24. Pelleg, J.; Zevin, L.Z.; Lungo, S.; Croitoru, N. Reactive-sputter-deposited TiN films on glass substrates. *Thin Solid Film.* **1991**, *197*, 117–128. [CrossRef]
25. Xu, Z.; Zhang, Z.; Bartosik, M.; Zhang, Y.; Mayrhofer, P.H.; He, Y. Insight into the structural evolution during TiN film growth via atomic resolution TEM. *J. Alloys Compd.* **2018**, *754*, 257–267. [CrossRef]
26. Mayrhofer, P.H.; Geier, M.; Löcker, C.; Chen, L. Influence of deposition conditions on texture development and mechanical properties of TiN coatings. *Int. J. Mater. Res.* **2009**, *100*, 1052–1058. [CrossRef]
27. Salamania, J.; Johnson, L.J.S.; Schramm, I.C.; Calamba, K.M.; Boyd, R.; Bakhit, B.; Rogström, L.; Odén, M. Influence of pulsed-substrate bias duty cycle on the microstructure and defects of cathodic arc-deposited $Ti_{1-x}Al_xN$ coatings. *Surf. Coat. Technol.* **2021**, *419*, 127295. [CrossRef]
28. Shugurov, A.R.; Nikonov, A.Y.; Dmitriev, A.I. The effect of electron-beam treatment of the deformation behavior of EBAMTi-6Al-4V under scratching. *Facta Univ. Ser. Mech. Eng.* **2022**, 1–13. [CrossRef]
29. Kobayashi, M.; Doi, Y. TiN and TiC coating on cemented carbides by ion plating. *Thin Solid Film.* **1978**, *54*, 67–74. [CrossRef]